Important Notice to Authors

Attached is a PDF proof of your forthcoming article in Optics Express. The article Manuscript ID is 395648. *No further processing of your paper will occur until we receive your response to this proof.*

Note: *Excessive proof corrections submitted by the author can result in significant delays to publication. Please include only essential changes that might be needed to address any shortcomings noticed in the proof-preparation process.*

Author Queries

Please answer these queries by marking the required corrections at the appropriate point in the text or referring to the relevant line number in your PDF proof.

Q1	The funding section is reserved for funder names and awards for searchability. To include the exact wording you provided, we created a new paragraph in the Acknowledgments section. If you would like to update the list of funders/awards, then please let us know. We can update the information in Prism and include the new funders/awards in the Funding section.
Q2	The funding information for this article has been generated using the information you provided to OSA at the time of article submission. Please check it carefully. If any information needs to be corrected or added, please provide the full name of the funding organization/institution as provided in the Crossref Open Funder Registry (https://search.crossref.org/funding).

Other Items to Check

- Please note that the original manuscript has been converted to XML prior to the creation of the PDF proof, as described above. The PDF proof was generated using LaTeX for typesetting. The placement of your figures and tables may not be identical to your original paper.
- Please carefully check all key elements of the paper, particularly the equations and tabular data.
- Author list: Please make sure all authors are presented, in the appropriate order, and that all names are spelled correctly.
- If you need to supply new or replacement figures, please place the figures in a Word or LaTeX manuscript template at the desired final figure size. Upload a PDF version of the document with figures when submitting proof corrections.

Research Article | Vol. 0, No. 0 / 00 00 0000 / Optics Express 1

Optics EXPRESS

Optical proxy for particulate organic nitrogen from BGC-Argo floats

Alain Fumenia,[1,5] Anne Petrenko,[1,6] Hubert Loisel,[2] Kahina Djaoudi,[3] Alain deVerneil,[4] and Thierry Moutin[1]

[1]*Aix Marseille Université, Université de Toulon, CNRS, IRD, OSU PYTHEAS, Mediterranean Institute of Oceanography (MIO), UM 110, 13288, Marseille, Cedex 09, France*
[2]*Univ. Littoral Côte d'Opale, CNRS, Univ. Lille, UMR 8187 - LOG - Laboratoire d'Océanologie et de Géosciences, F-62930 Wimereux, France*
[3]*University of Arizona, department of Molecular and Cellular Biology, 1007 E Lowell Street Life Science South, room 315 Tucson, AZ 85721, USA*
[4]*The Center for Prototype Climate Modeling, New York University Abu Dhabi, Abu Dhabi, United Arab Emirates*
[5]*alain.fumenia@mio.osupytheas.fr*
[6]*anne.petrenko@mio.osupytheas.fr*

Abstract: Using biogeochemical-Argo float measurements, we propose, for the first time, an optical proxy for particulate organic nitrogen concentration (PON) in the Western Tropical South Pacific, an area influenced by dinitrogen (N_2) fixation. Our results show a significant relationship between the backscattering coefficient at 700 nm (b_{bp}) and PON, especially when the latter is measured using the wet oxidation method (R^2=0.87). b_{bp} may be used to estimate PON concentrations (PON^{opt}) between 0.02 and 0.95 µM, allowing for unprecedented monitoring using autonomous profiling floats. The b_{bp} *vs* PON relationship can be used to study phytoplanktonic biomass dynamics at relevant seasonal temporal scales, with clear evidence of PON^{opt} as a proxy of phytoplanktonic biomass, at least for this specific area. Temporal analyses of PON^{opt} show significant increases (from 0.16 to 0.80 µM) likely related to new production associated to N_2 fixation events measured during stratification periods in the Melanesian Archipelago.

1. Introduction

The surface waters of the subtropical South Pacific gyre (SPG) are permanently depleted in dissolved inorganic nitrogen (NO_3^-) [1], making this area the largest oceanic desert in the world's ocean [2]. However, in some oligotrophic areas, biological N_2 fixation offers the marine phytoplankton community a mechanism to relieve nitrogen limitation in the euphotic surface layer [3,4]. In the framework of the Oligotrophy to UlTra-oligotrophy PACific Experiment (OUTPACE) cruise (19 Feb-3 Apr 2015), record N_2 fixation rates were recently observed in the upper waters of the Western Tropical South Pacific (WTSP) at the end of austral summer [5]. Despite a NO_3^- depleted mixed layer, a significant increase of phytoplanktonic biomass was observed during N_2 fixation events. However, the limited observations of seasonal phytoplankton biomass dynamics, hypothesized to be largely driven by N_2 fixation [6,7], considerably restricts our understanding of the WTSP's biogeochemical functioning. To overcome present limitations, *in situ* observations over a broad range of time scales are required.

Biogeochemical-Argo (BGC-Argo) profiling floats are capable of autonomously observing bio-optical properties such as Chlorophyll-*a* (Chl*a*) fluorescence and particulate backscattering coefficient (b_{bp}) at high frequency [8]. The use of bio-optical proxies has been previously shown to have high reliability in the estimation of biogeochemical variables such as Chl*a* and particulate organic carbon (POC), among others [8,9]. While Chl*a* fluorescence is the most commonly used proxy for living phytoplankton cells [10,11], b_{bp} variability is instead driven by both the algal

#395648 https://doi.org/10.1364/OE.395648
Journal © 0000 Received 23 Apr 2020; revised 19 Jun 2020; accepted 19 Jun 2020; published 00 00 0000

Optics EXPRESS

and non-pigmented particle pools including viruses, heterotrophic bacteria, and non-living cells in case 1 oceanic waters [12]. For this reason, b_{bp} has long been used as a proxy of POC in open ocean water in the absence of mineral particles [9,12–19].

In oligotrophic areas, the carbon hydrogen nitrogen (CHN) method requires a high volume of filtered seawater, up to 10 L, to obtain accurate POC measurements [19]. Filtering such volumes of sea water is extremely time consuming and limits throughput of large numbers of samples. Several factors can lead to large biases in estimated POC in oligotrophic areas, including contamination, adsorption of dissolved organic carbon (DOC) onto filters, particle formation in bottle samples after collection, the contribution of particulate inorganic carbon, as well as particle retention, among others [19–22]. Particulate organic nitrogen and phosphorus measurements obtained by the wet oxidation method ($PON_{(wet)}$ and $POP_{(wet)}$, respectively) could represent a valuable alternative in oligotrophic areas, since the method's sensitivity requires smaller volumes of seawater than the CHN method [23], making it less sensitive to the potential contaminations alluded to above. Wet oxidation requires a maximum volume of 1.2 L, even in oligotrophic areas. The smaller volume and the absence of an acidification step to remove inorganic particles on the filter significantly decrease both the time required for each sample and potential particle formation as transparent exopolymer particles (TEP; 22) in bottle samples, thus decreasing potential contamination.

The wet oxidation method has been shown to be more accurate than the CHN method for PON and POC measurements [23]. Based on the fact that POC and PON generally covary [1,6], one may expect a good correlation between b_{bp} and PON. As a result, the use of an optical proxy of PON (PON^{opt}) could provide a means to estimate seasonal variations of phytoplanktonic biomass and associated particles, especially in oligotrophic areas.

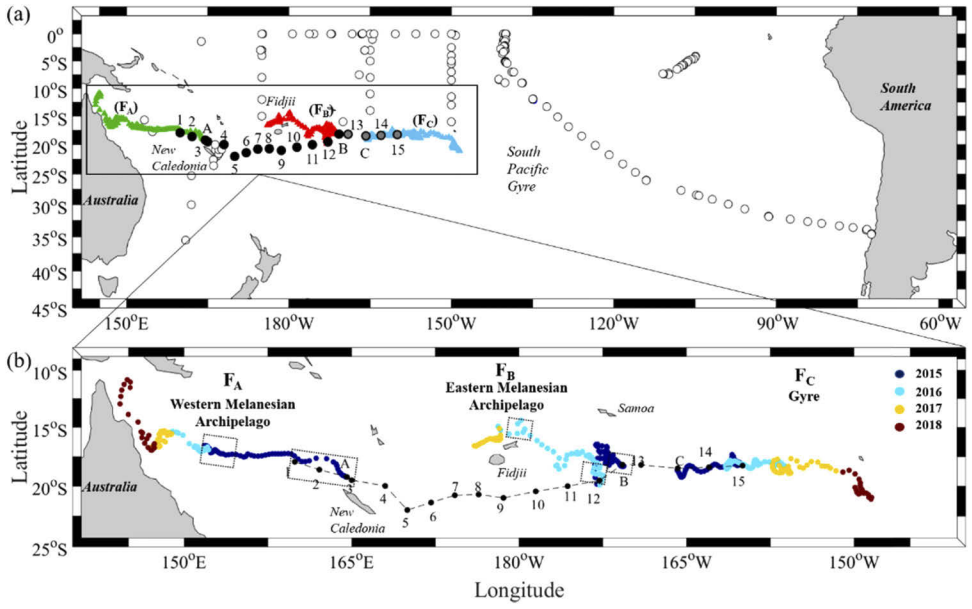

Fig. 1. (a) Trajectory of the BGC-Argo floats deployed in this study (green triangle = F_A, red triangle = F_B, blue triangle = F_C). The location of the OUTPACE section is represented by black (Western and Eastern Melanesian Archipelago) and grey (South Pacific gyre) circles. Open circles represent the location of available *in situ* PON measurements in the South Pacific [24]. (b) Zoom on the trajectory of the BGC-Argo floats. Colors represent the time (years) and the black dashed boxes show the "bloom periods" defined in the text.

Optics EXPRESS

In areas where nitrogen is the key limiting nutrient, and N_2 fixation is sufficiently favored, both an increase in PON standing stocks and a tight coupling between N_2 fixation and surface water PON accumulation have been observed [24,25]. While PON estimates allow one to follow phytoplanktonic biomass, observations in the South Pacific are sparse [26] [Fig. 1(a)], stressing the need to develop indirect methods for estimating this key variable at regional and pertinent time scales. For this purpose, three BGC-Argo floats were deployed during the OUTPACE cruise. Our study focuses on the mixed layer, where the N_2 fixation process mainly occurs [25]. The main goals of this work are (1) to characterize and discuss, for the first time, b_{bp}*vs* PON relationships to define an optical proxy of PON (PON^{opt}), and then, (2) to investigate the seasonal dynamics of the particulate organic biomass in the WTSP, an area influenced by N_2 fixation events, using Chl*a* and PON^{opt} seasonal distributions.

2. Materials and methods

The OUTPACE cruise took place along a West to East transect [Fig. 1(b)]. A total of 18 stations were sampled from the oligotrophic water of the Western and Eastern Melanesian Archipelago (WMA and EMA, respectively) to the clearest ocean waters of the SPG [27].

PON and particulate organic phosphorus (POP) samples were collected at 16 depths between the surface and 500 m from a SBE 911+ CTD-Rosette in polycarbonate bottles. PON and POP concentrations were quantified spectrophotometrically following the wet oxidation method ($PON_{(wet)}$ and $POP_{(wet)}$) based on persulfate digestion at 120 °C [28]. Following this method, a volume of 1.2 L was filtered through a pre-combusted (24 h, 450 °C) 47 mm GF/F filter. The filter was then placed in a Teflon bottle in which 20 mL of milli-Q water and 2.5 mL of the oxidizing reagent were previously dispensed (concentration factor: 1.2/0.0225). Nitrate and phosphate concentrations were then determined in the digested sample using an automated colorimetric procedure on a Technicon auto-analyzer [29]. The repeatability, calculated as the coefficient of variation (CV) for $PON_{(wet)}$ and $POP_{(wet)}$ field-collected replicates (n=10), was 2% and 3%, respectively. The accuracy, linked to the uncertainty of the calibration curve's slope (calculated as the CV of the slope) of $PON_{(wet)}$ and $POP_{(wet)}$ was 1.46% and 1.36% (n=14), respectively. For each station, pre-combusted GF/F filters were used on board as sample blanks. The blank consisted of adding the same volume of oxidizing reagent to 20 mL of milli-Q water, in which a pre-combusted GF/F filter was previously added. The means of filter blanks of $PON_{(wet)}$ and $POP_{(wet)}$ were 0.036 ± 0.002 µM and 0.0021 ± 0.0001 µM. The quantification limits of $PON_{(wet)}$ and $POP_{(wet)}$, calculated as ten times the standard deviation of 10 blank measurements [30], were 0.02 µM and 0.001 µM, respectively. The maximum quantification limits for $PON_{(wet)}$ and $POP_{(wet)}$ were [PON]max = [standard NO_3^-]max/(concentration factor) = 0.95 µM and [POP]max = [standard PO_4^{3-}]max/(concentration factor) = 0.060 µM, respectively. Mineralization efficiencies measured daily with P-choline and urea standards were 100 ± 2% for N and 99 ± 1% for P (n=27).

A second set of PON measurements used a PerkinElmer 2400 CHN analyzer ($PON_{(CHN)}$), with standards prepared with a 20 g L^{-1} glycine (VWR C14037000) solution (N range: 0.15-10 µM). Seawater samples (2 L) were filtered through pre-combusted (4 h, 450° C) 25 mm GF/F filters, dried at 60° C and stored in 1.5 mL Eppendorf PE tubes. The repeatability for $PON_{(CHN)}$ field-collected replicates (n=6) was 4.60% and the calibration curve slope CV was 2.83% (n=13). For each station, pre-combusted GF/F filters were used on board as sample blanks. These filter blanks were processed in the same way as sample filters without the filtration step. The mean of filter blanks of $PON_{(CHN)}$ was 0.021 ± 0.014 µM. The quantification limit of $PON_{(CHN)}$ was 0.13 µM. $PON_{(wet)}$ and $PON_{(CHN)}$ concentrations showed an excellent agreement (R^2=0.92; slope = 1.03 ± 0.03). The recovery between $PON_{(CHN)}$ and $PON_{(wet)}$ is close to 100% (95% C.I of the slope = [0.96 1.11]; 95% C.I of the intercept = [-0.03 0.028]) with a very low standard deviation over the range of concentrations measured as part of this study, highlighting that the

Optics EXPRESS

wet oxidation method recovered all the PON from living phytoplankton and associated particles as previously reported by [23,31].

Three BGC-Argo floats (F_A), (F_B) and (F_C) were deployed in March/April 2015 near the stations LDA, LDB and LDC respectively [Fig. 1(b)], and their collected data were downloaded from the Coriolis database website (ftp://ftp.ifremer.fr/ifremer/argo/dac/coriolis/). These floats were equipped with a Sea-Bird Electronics (SBE41CP) conductivity-temperature-depth (CTD) sensor (Seabird Inc., USA) and an additional sensor package: the WETLabs Environmental Characterization Optics triplet puck (ECO3, Seabird Inc., USA) measuring the fluorescence of Chl*a* at excitation/emission wavelengths of 470/695 nm and the angular backward scattering coefficient of particles at 700 nm (Table 1).

Table 1. Equipment details for each float used in this study, (the first fifteen, nineteen, and eleven profiles were recorded every day for floats F_A, F_B and F_C, respectively, before starting to sample every five days).

	F_A	F_B	F_C
Argo float number	6901656	6901658	6901660
Number of profiles	186	146	178
Dates of measurements	03/03/2015 - 07/27/2018 (1243 days)	03/21/2015 - 07/13/2017 (846 days)	03/29/2015 - 07/24/2018 (1235 days)
Deployment	19.13° S/164.29° W	18.16° S/170.43° W	18.28° S/165.46° W
The closest CTD (Stations)	CTD 067 (LDA)	CTD 151 (LDB)	CTD 199 (LDC)
Dates of the CTD	03/03/2015	03/20/2015	03/28/2015
Distance (km) between stations and float data used in matchups	14.9	9.7	2.9
Parameters used in this study	Latitude, Longitude, Time (days), Pressure (dbar), Salinity, Temperature (°C), Chl*a* (mg m^{-3}), b_{bp} (m^{-1})		

Measurements were collected every 1 or 5 days between 1,000 dbar and the surface, with a sampling resolution of 1 dbar between the surface (0.1-1 dbar) and 250 dbar and 10 dbar between 250 and 500 dbar, respectively. Growth rate of diazotrophs like *Trichodesmium* (the main diazotroph in the WTSP) are generally low and blooms last for months, indicating that 5 days is a correct sampling time to capture a diazotroph bloom. The data were quality controlled following the standard Argo protocol [32–34].

Mixed layer depth (MLD) was calculated using a threshold density of 0.03 kg m^{-3} deviation from the reference value at 10 m depth [35].

The fluorescence measurements of Chl*a* were converted to Chl*a* concentrations according to the procedure detailed by [33]. Chl*a* concentrations were cleaned from out-of-range values and, following the recommendations of [36], adjusted Chl*a* concentrations were divided by a factor of two. A non-photochemical quenching correction was applied following the standard Argo protocol [33]. Vertical profiles of Chl*a* concentrations showed that most of the Chl*a* values observed in deep waters (> 200 dbar) were negative (figure not shown). To correct the negative deep Chl*a* concentrations, we removed a constant value (the deepest Chl*a* fluorescence value from the profile, i.e., so-called "deep-offset correction"). During the OUTPACE cruise, a "Fluorimeter, Chelsea Aquatracka MKIII" attached to a SeaBird CTD rosette was used to measure the Chl*a* fluorescence. Calibration of the fluorimeter was carried out using HPLC Chl*a* measurements from 13 OUTPACE stations (stations SD1, LDA, SD6, SD8, SD10, SD12, LDB, LDC, SD14, SD15), hence just before the BGC-Argo deployments. Very good agreement ($p>0.01$, Fig. 2) was observed between the first vertical profile of adjusted Chl*a* concentrations and the vertical profile of Chl*a* concentrations measured *in situ* at the closest OUTPACE CTDs in time and space (Table 1).

Optics EXPRESS

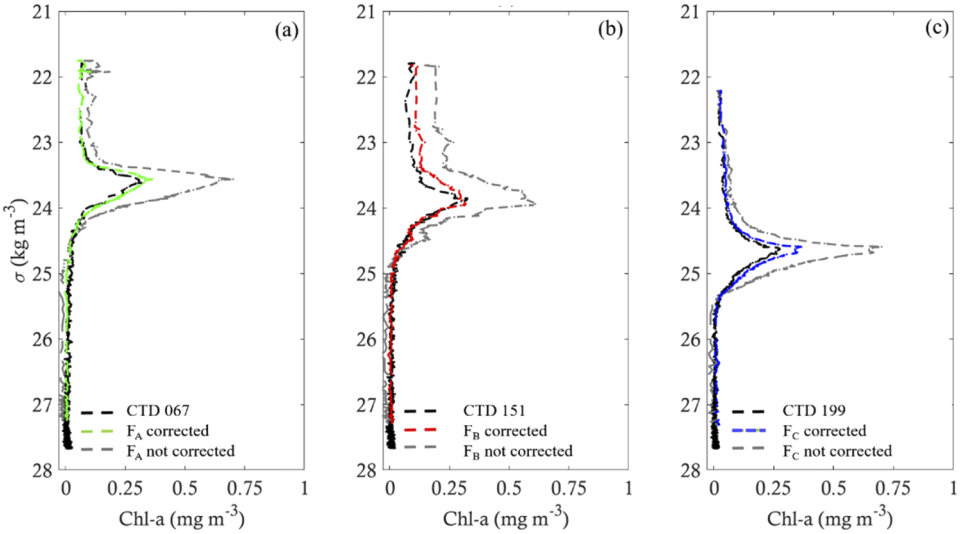

Fig. 2. (a, b, c) Comparison between the respective concentrations of Chl*a* (mg m^{-3}) measured by the CTD 067/151/199 (black dashed lines), uncorrected Chl*a* (mg m^{-3}) concentrations measured by floats F_A / F_B / F_C (gray lines), and corrected (colored lines) Chl*a*, depending on the density (kg m^{-3}).

The backscattering sensors measure the angular scattering coefficient at 124° relative to the direction of light propagation at a wavelength of 700 nm. This measurement is then transformed into the b_{bp} following [34], using the conversion factor of [37] ($\chi = 1.076$). Negative values of b_{bp} were removed and vertical profiles were quality-controlled following the standard Argo protocol [34]. Both datasets (Chl*a* and b_{bp}) have indeed been checked qualitatively and no sensor drift or bio-fouling have been observed.

The variability of b_{bp} with PON is investigated between the surface and 500 dbar using the OUTPACE CTD-rosette water samples, which were the closest in time and space to the float profiles where b_{bp} was measured (Table 1). To avoid the effect of internal waves, each bottle data value was paired with a b_{bp} value at the same density coordinate. Differences in density between the bottle data and associated b_{bp} values were found to be less than 0.005 kg m^{-3}.

3. Results

3.1. *From backscattering to particulate organic matter*

The b_{bp} *vs* PON relationship is investigated to understand the extent to which b_{bp} can be used as a proxy of PON to better assess the impact of N_2 fixation events at the relevant seasonal temporal scales. Here we investigate the b_{bp} *vs* PON relationship (1) in the mixed layer (ML), (2) in the ML and the deep Chl*a* maximum (DCM) [0-150 dbar, Fig. 3(b)], and (3) in the whole sampled water column (0-500 dbar), before deriving PON^{opt} and POP^{opt}.

All $PON_{(wet)}$ concentrations and most of the $PON_{(CHN)}$ concentrations are above their respective quantification limits. By considering these data, a significant relationship is obtained between b_{bp} and PON, regardless of the experimental method used to measure PON (wet *vs* CHN) (Fig. 3; Table 2). The b_{bp} *vs* $PON_{(wet)}$ relationship is better than that of b_{bp} *vs* $PON_{(CHN)}$ between the surface and 150 (500) dbar [Figs. 3(c), 3(d); Table 2]. Methodologically based variability could explain this discrepancy. Indeed, the wet oxidation method achieves a sensitive measurement from a smaller volume (1.2 L) of seawater than the CHN method (2-10 L), making this method highly sensitive and suitable for PON analyses in oligotrophic waters [6,28].

Optics EXPRESS

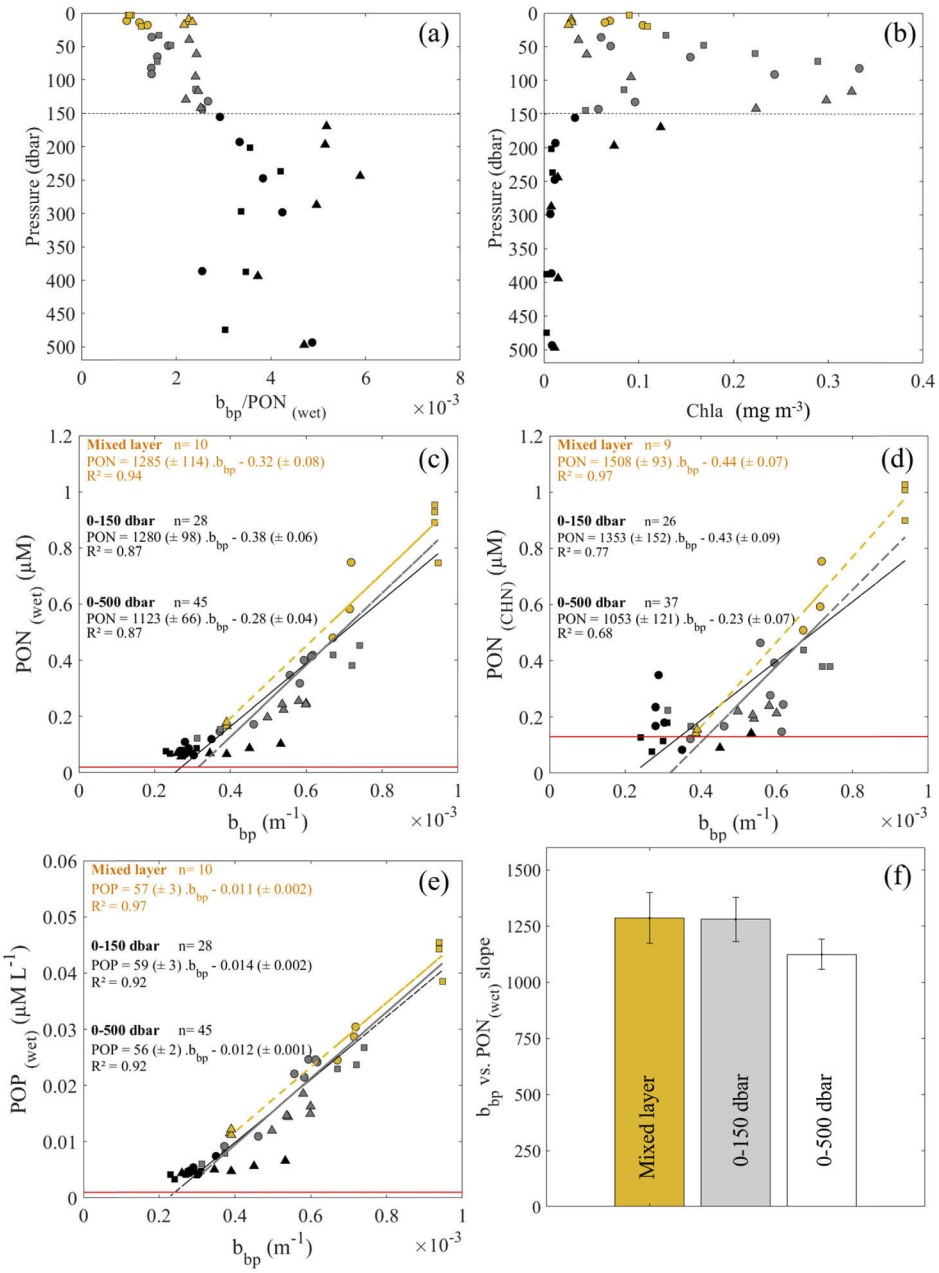

Fig. 3. (a) Ratio of $b_{bp}/PON_{(wet)}$ *vs* Pressure, (b) Chl*a* concentrations *vs* Pressure, and scatter plots between b_{bp} (m^{-1}) measured during the first profiles of the F_A, F_B and F_C floats and (c) $PON_{(wet)}$, (d) $PON_{(CHN)}$, and (e) $POP_{(wet)}$. (The yellow, grey, and black lines represent the best linear regression fits for the data points in the ML, 0-150 dbar, and 0-500 dbar, respectively). Mixed layer = yellow markers/yellow lines, 0-150 dbar = yellow + grey markers/ grey lines, 0-500 dbar = yellow + grey + black markers/ black lines. (f) b_{bp} *vs* $PON_{(wet)}$ slopes in the mixed layer, between the surface and 150 dbar, and between the surface and 500 dbar (note: circle = F_A/LDA, square = F_B/LDB, triangle = F_C/LDC). Red lines correspond to quantification limits. Statistical parameters are in Table 2.

Optics EXPRESS

Table 2. Statistical parameters for b_{bp} *vs* $PON_{(wet)}$, $PON_{(CHN)}$, and $POP_{(wet)}$ for the three depth categories: 0-500 dbar, 0-150 dbar, and Mixed Layer. n is the number of data points, R^2 is the determination coefficient, RMSE the Roots Mean Square Error (µM), Median of residuals (residuals = observed minus fitted values), and 75th and 25th percentile represents the interquartile range of residuals).

	b_{bp} *vs* $PON_{(wet)}$	b_{bp} *vs* $PON_{(CHN)}$	b_{bp} *vs* $POP_{(wet)}$
	0-500 dbar		
n	45	37	45
R^2	0.87	0.68	0.92
p-value	< 0.001	< 0.001	< 0.001
RMSE	0.09	0.143	0.003
Median of residuals	0.01	0.03	0.001
75th percentile	0.05	0.11	0.002
25th percentile	-0.06	-0.13	-0.002
	0-150 dbar		
n	28	26	28
R^2	0.87	0.77	0.92
p-value	< 0.001	< 0.001	< 0.001
RMSE	0.09	0.13	0.003
Median of residuals	0.01	0.03	<0.001
75th percentile	0.06	0.06	0.003
25th percentile	-0.07	-0.11	-0.003
	Mixed layer		
n	10	9	10
R^2	0.94	0.97	0.97
p-value	< 0.001	< 0.001	< 0.001
RMSE	0.082	0.063	0.002
Median of residuals	0.004	0.005	<0.001
75th percentile	0.04	0.003	0.002
25th percentile	-0.02	-0.05	-0.001

The $b_{bp}/PON_{(wet)}$ ratios exhibit a low variability with depth, with an average value of $1.9 \times 10^{-3} \pm 5.7 \times 10^{-4}$ m^{-1} μM^{-1} [Fig. 3(a)] in the layer including the ML and the DCM, [Fig. 3(b)]. In the ML, the slope derived from the b_{bp} *vs* $PON_{(wet)}$ relationship [1285 ± 114; Figs. 3(c), 3(f)] is not significantly different from that observed in the 0-150 dbar layer [1280 ± 98; Fisg. 3(c), 3(f)]. In contrast, below the DCM (>150 dbar), an increase in $b_{bp}/PON_{(wet)}$ ratios is observed, with an average value reaching $4.1 \times 10^{-3} \pm 9.5 \times 10^{-4}$ m^{-1} μM^{-1} [Fig. 3(a)]. The slope from the b_{bp} *vs* $PON_{(wet)}$ relationship obtained between 0 and 500 dbar is significantly lower than those observed in both the ML and between the surface and 150 dbar [Fig. 3(f)].

Hereafter, to investigate the temporal variability of phytoplanktonic biomass and associated particles in the WTSP, the b_{bp} measurements will be discussed in terms of PON using the relationship established from the b_{bp} and $PON_{(wet)}$ data set measured between the surface and 150 dbar [Fig. 3(c)] [Eq. (1)].

$$PON^{opt} = 1280 \times b_{bp}(700) - 0.38 \ (\mu M) \quad (1)$$

Studying each float separately in the 0-150 m layer, the b_{bp} *vs* $PON_{(wet)}$ relationships are only significant for F_A and F_B, with similar slopes (p<0.001) (Table 3). The F_C/LDC data are very

Optics EXPRESS

few (n=9) and F_C exhibits low and quasi-constant $PON_{(wet)}$ values. We therefore decide not to calculate the b_{bp} *vs* PON relationship for the LDC station individually. Nevertheless, including F_C/LDC data in the global b_{bp} *vs* $PON_{(wet)}$ relationship does not significantly affect the slope (Table 3), so the global relationship is therefore calculated with all the data in the 0-150 m layer.

Table 3. Slopes and intercepts for the b_{bp} *vs* $PON_{(wet)}$ and b_{bp} *vs* $POP_{(wet)}$ relationships for F_A-F_B/LDA-LDB, and $F_A/F_B/F_C$ in the 0-150 m layer. (R^2 = the determination coefficient, p is the p-value).

	Floats	Slopes	Intercepts	R^2	p-value	n
b_{bp} *vs* $PON_{(wet)}$	F_A/F_B	1277 ± 111	-0.36 ± 0.08	0.89	p < 0.001	19
	F_C	Not calculated				
	$F_A/F_B/F_C$	1280 ± 98	-0.38 ± 0.06	0.87	p < 0.001	28
b_{bp} *vs* $POP_{(wet)}$	F_A/F_B	59 ± 3	-0.01 ± 0.002	0.95	p < 0.001	19
	F_C	Not calculated				
	$F_A/F_B/F_C$	59 ± 3	-0.01 ± 0.002	0.92	p < 0.001	28

We consider the intercept of the $PON_{(wet)}$ *vs* b_{bp} relationship as the lower detection limit of b_{bp} to derive PON^{opt}. The highest value of b_{bp} for which this equation is valid corresponds to the maximum value measured. Values of b_{bp} for which the b_{bp} *vs* $PON_{(wet)}$ relationship is valid range between 3.4×10^{-4} and 9.5×10^{-4} m^{-1}. Additionally, values of b_{bp} for which the b_{bp} *vs* $POP_{(wet)}$ relationship is valid range between 2.7×10^{-4} and 9.5×10^{-4} m^{-1}.

3.2. Mixed layer depth and chlorophyll-a seasonal distribution

In general, the seasonal Chl*a* patterns mimic the MLD seasonal variability, with low mixed layer values observed during the summer (January/February/March) and high values during the winter (July/August) (Fig. 4). However, in the WMA (F_A), increases of Chl*a* at shorter time scales were superimposed onto the seasonal pattern, with values reaching 0.09 mg m^{-3} in March/April 2015 and 0.10 mg m^{-3} in October/November 2015. These episodes were not related to abrupt changes in the MLD but occurred during conditions of shallow MLD (< 60 dbar) [dashed frame on Fig. 4(a)]. In the EMA (F_B), Chl*a* followed the same seasonal variations as observed in 2016 and 2017 in the WMA (F_A), except for the summer period: despite a shallow MLD (< 45 dbar), Chl*a* showed relatively high values, reaching 0.14 mg m^{-3} in March/April 2015, 0.08 mg m^{-3} in January/February 2016, and 0.10 mg m^{-3} in February 2017 [dashed frame on Fig. 4(c)]. The absence of intense vertical mixing and relatively high light levels (figure not shown) during these stratified periods should result in a diminution of the Chl*a* concentrations. Observing the opposite, we hypothesize that the high Chl*a* concentrations point to an additional controlling factor of the variability of Chl*a* dynamics in the area, probably linked to diazotroph blooms.

3.3. PON seasonal distribution

In contrast to Chl*a*, the temporal evolution of PON^{opt} was relatively even, with low values generally below 0.20 µM (Fig. 4). However, as for Chl*a*, increases of PON^{opt} were observed during the first year in the WMA (F_A) and each year at particular times, between January and April, in the EMA (F_B). Indeed, in the WMA (F_A), between January 2016 and July 2017, despite the seasonal cycle of Chl*a*, PON^{opt} was constant over time [Fig. 4(b)], with an average value of 0.18 ± 0.06 µM over this period [Fig. 4(b)]. Conversely, PON^{opt} values were significantly higher ($p<0.01$, t-test) in 2015 than those observed in 2016 and 2017 [Fig. 4(b)]. Maximum values were recorded during March/April 2015 and October/November 2015, averaging 0.41 ± 0.09 µM during both periods [dashed frames on Fig. 4(b)], simultaneous with increases of Chl*a* [dashed frames on Fig. 4(a)].

Optics EXPRESS

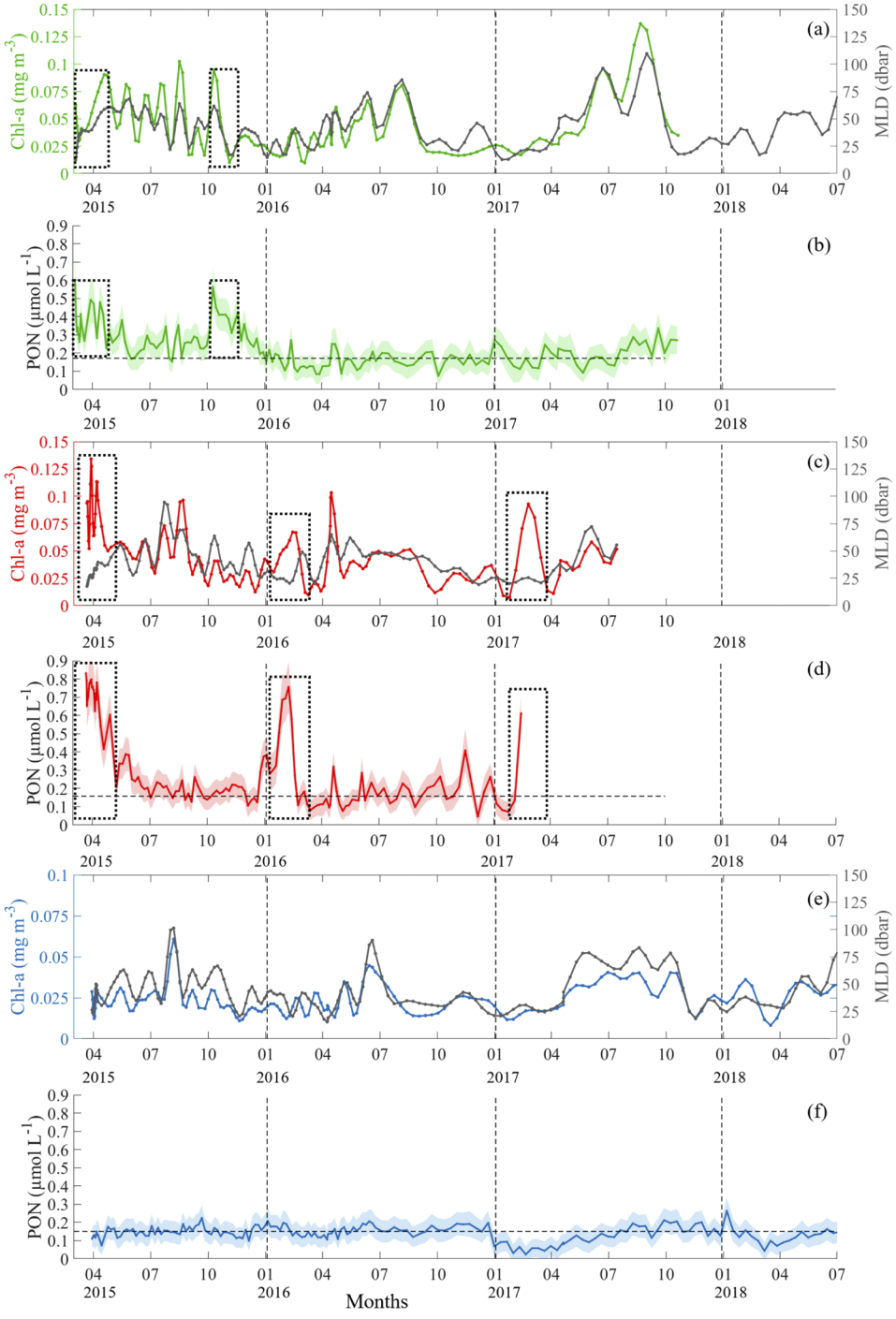

Fig. 4. Temporal variations of the mixed layer depth (dbar) (black line) and the mixed layer average Chl*a* (mg m^{-3}) concentration for floats (a) F_A (green line), (c) F_B (red line), and (e) F_C (blue line), along with temporal variations of (b) the mixed layer average PON^{opt} concentration (µM) (± sd) for float F_A (green line), (d) float F_B (red line), and (f) float F_C (blue line). Lighter colors show standard deviation around the mean (the uncertainty in the regression has been incorporated into the error propagation). Black dashed frames show the "bloom periods" as defined in the text.

Optics EXPRESS

In the EMA (F_B) during the summer periods, the average PON^{opt} values reached 0.70 ± 0.10 µM during March/April 2015, 0.50 ± 0.20 µM during January/February 2016 and 0.60 ± 0.03 µM during February 2017 [dashed frames on Fig. 4(d)], coinciding with relatively strong increases of Chl*a* [dashed frames on Fig. 4(c)]. Outside of these summer periods, PON^{opt} values were mostly constant with an average value of 0.17 ± 0.06 µM [Fig. 4(d)], similar to F_A in 2016/2017. In the SPG (F_C), no increases of PON^{opt} were observed during the summer period. Instead, PON^{opt} was constant throughout the study period, with an average value of 0.16 ± 0.04 µM [Fig. 4(f)].

Hereafter, periods with both significant increases of PON^{opt} by a factor of 5 (from 0.16 to 0.80 µM) and Chl*a* by a factor of 4 to 5 (from 0.03 to 0.14 mg m^{-3}) are called 'bloom periods' [dashed frames on Fig. 1(b) and Fig. 4]. These periods are: March/April 2015 and October/November 2015 for F_A, and March/April 2015 and January/February 2016 and February 2017 for F_B.

4. Discussion

At first order, b_{bp} variability is driven by the concentration of bulk particulate matter, with changes in the particulate size distribution, refractive index, and particle morphology, among other factors, generally acting at second order [12]. The inherent optical properties (IOP) values relative to the concentration (or mass) of biogeochemical parameters (here $b_{bp}/PON_{(wet)}$) are sensitive to these second-order effects. While a relatively constant $b_{bp}/PON_{(wet)}$ ratio indicates homogeneous bulk particulate matter in terms of backscattering efficiency in the surface layer, an increase at depth indicates modification and/or heterogeneity of bulk particulate matter. Our result suggests that the influence of different particle composition and/or a potential presence of distinct microbial communities observed during the OUTPACE cruise (diazotrophic organisms in the ML and DCM microbial communities below the ML, [25,38]) was not significant compared to changes in organic particulate concentration. Thus, it seems that biomass changes are a dominant source of b_{bp} variability, as previously reported by [39]. These observations are also in agreement with those of [19], who reported that the POC *vs* b_{bp} relationship was relatively insensitive to community composition. In contrast, below the DCM (>150 dbar), an increase in $b_{bp}/PON_{(wet)}$ ratios is observed. This finding could reflect the presence of an assemblage of particles dominated by detritus and heterotrophs (but requires further analysis based on a better characterization of the bulk particulate matter below the DCM). The main conclusion of these observations is that the highly sensitive wet oxidation method provides a good b_{bp} *vs* $PON_{(wet)}$ relationship for this area between the surface and 150 dbar, and valid between 0.02 and 0.95 µM (~50-fold biomass increase), which thanks to float-based measurements of b_{bp} can be leveraged to expand both the number of observations and the spatiotemporal scales resolved.

During the periods of no bloom in the Melanesian Archipelago, and throughout the study period in the SPG, PON^{opt} concentrations were remarkably stable and low (<0.20 µM), displaying a net balance between production (or supply) and remineralization (or removal) processes [24]. The relative increase of Chl*a* and the constant values of PON^{opt} during the winter periods suggest a seasonal change in Chl*a* cell quota due to a lower light intensity in winter coupled with deeper mixed layer depths [40,41]. As a result, the constant PON^{opt} suggests that the marked Chl*a* seasonal cycle, which can be falsely interpreted as a biomass variation, is in fact not related to new production but is instead a steady phytoplankton biomass. In our study region, the absence of phytoplanktonic blooms could be linked to nitrogen limitation [1], while N_2 fixation could be constrained by lower iron availability [42,43].

During the bloom periods of the austral summer, coinciding with the increase of Chl*a* concentrations, PON^{opt} concentrations increased by a factor of two to five only in the Melanesian Archipelago. A co-variation between Chl*a* concentrations and b_{bp} values (or PON^{opt} in our case) is linked to phytoplankton biomass production [44–47]. The results obtained in this study extend this observation to subtropical areas, pointing to outstanding increases of living phytoplanktonic

Optics EXPRESS

biomass and associated particles, even in oligotrophic regions. To explain the recurrent increases of phytoplanktonic biomass during austral summer periods, it is necessary to identify the nitrogen sources in the mixed layer. The two first blooms (March/April 2015 for both F_A and F_B) reported in this study occurred during the OUTPACE cruise. During those blooms, high N_2 fixation rates were reported while NO_3^- was extremely low. Regarding the diazotroph bloom observed at station LDB, mesoscale vertical fluxes were too weak to displace the nitracline [48]. As a result, delivered nitrogen to the surface from mesoscale activity could not sustain the observed primary production. Regarding the blooms observed in our study after the cruise, except during February 2017 in the EMA no significant decreases of salinity were measured in parallel to PON^{opt} increases over the study period [Fig. 5], suggesting no direct influence of precipitation or riverine inputs.

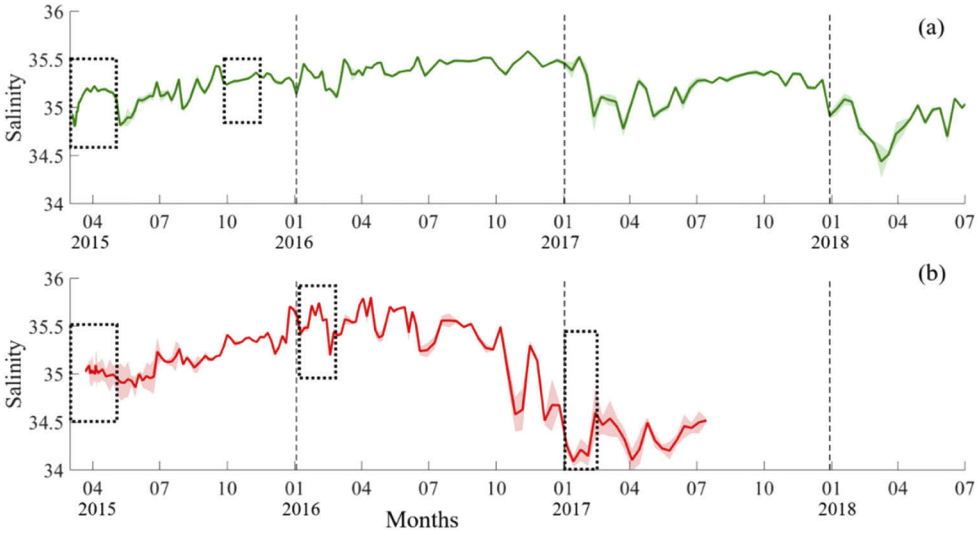

Fig. 5. Temporal variations of (a) the average salinity (±sd) in the mixed layer for float F_A (green line) and (b) float F_B (red line). Black dashed frames show the "bloom periods" defined in the text.

Furthermore, atmospheric particle deposition fluxes are very low in the region [49]. The top of the nitracline was 90 dbar in the area during the summer [6], significantly deeper than the measured MLD (<60 dbar, Fig. 4). However, physical processes could vertically displace isopycnals tens of meters along with the nitracline [50]. Nevertheless, extreme events such as cyclones reported in this area perturbed the phosphacline but not the deeper nitracline, resulting in surface increases of phosphate but not of nitrate [51]. Therefore, in the absence of vertical N supply, the variations of PON^{opt} appear to be a valuable proxy of new production related to intense N_2 fixation events during austral summer conditions. In this specific environment characterized by active biological N_2 fixation, most of the new nitrogen is rapidly integrated into the phytoplanktonic biomass. Even if part of the nitrogen is released to the labile dissolved organic and inorganic pools, it is rapidly re-assimilated by the nitrogen-starved organisms [52,53]. We therefore conclude that the increases of PON^{opt} are most likely related to living POM, i.e. phytoplankton cells, and, to a lesser extent detritus.

In our study, we propose to use an optical proxy of PON rather than the traditional optical proxy of POC for several reasons. First, POC values show concentrations below 4 µM in oligotrophic gyres [54]. This limit value is close to the uncertainty reported in previous studies predicting POC from b_{bp} [9,19]. The use of PON would be a superior alternative as the wet oxidation procedure, coupled with spectrophotometric measurements, allows accurate quantification of

Optics EXPRESS

PON (quantification limit = 0.02 µM which correspond to 0.13 µM in terms of POC following the Redfield proportion), with reasonable volumes of filtered seawater (1.2 L). Second, oceanic primary production is primarily controlled by nitrogen availability [55,56]. Thus, it would be helpful, in order to better understand controls of primary production, to gain insight on nitrogen cycling, particularly on the seasonal cycle of nitrogen pools directly, rather than carbon pools. This argument is even more important to consider in environments characterized by active biological N_2 fixation [5] where N budgets are needed [6]. Theoretically, all essential elements may be used to track primary production rates and biomass accumulations. Relative to carbon, the ~30 essential nutrient elements display a range of plasticity in their cellular requirements [57], with N being the least plastic by varying in cellular N:C molar ratios from ~1/5 to 1/10, a factor of two [58]. This variability is low compared to changes in biomass at the scale of the world Ocean, and even in the oligotrophic WTSP [6]. Therefore, if biomass is dominated by phytoplankton, a close link between PON and POC is to be expected. Similarities notwithstanding, the relative ease of PON measurements in oligotrophic areas favors the use of a PON optical proxy.

In addition to $PON_{(wet)}$, the wet oxidation method can simultaneously measure $POP_{(wet)}$. Interestingly, the b_{bp} *vs* $POP_{(wet)}$ relationship was statistically better than b_{bp} *vs* $PON_{(wet)}$ [Fig. 3; Table 2], highlighting the possible use of POP as a biomass proxy, which would drive an accurate estimation of standing POP stocks and associated biogeochemical fluxes. The better relationship between POP and b_{bp} than PON and b_{bp} suggests that the bulk particulate matter of POP could be less optically variable than PON-bulk particulate matter. This result could be linked to the variability of particle composition between both PON and POP pools. One main signature of a given particulate organic matter pool is the relative contributions of living particles and detrital material. Turnover rates of POP have been previously shown to be significantly higher than POC in the subtropical south Pacific [59], with the carbon and nitrogen pools containing more refractory material than the phosphorus pool [60–62]. Consequently, POP was considered to contain a higher contribution of living particles than PON or POC [59]. Therefore, the significant b_{bp} *vs* $POP_{(wet)}$ relationship obtained [Fig. 3(c); Table 2] suggests that the variability of b_{bp} could be linked, at least for this study area, more to the abundance of phytoplanktonic biomass than to associated material, as previously reported by [63] and [64]. Consequently, the optical proxy of POP estimated from b_{bp} could also be a living biomass indicator and offer its own unique perspectives.

5. Conclusion

The combined use of *in situ* PON (and POP) measurements using the wet oxidation method, and optical properties measured by BGC-Argo floats close to *in situ* measurements, allowed to highlight, for the very first time, the excellent b_{bp} *vs* PON (and POP) relationships between 0 and 150 dbar in under-sampled oligotrophic waters. In such areas, the quantification of PON^{opt}, in the range between 0.02 and 0.95 µM, documents phytoplanktonic biomass dynamics (and associated properties) at the relevant seasonal temporal scale. Increases of PON^{opt} by a factor of 5 (from 0.16 to 0.80 µM) were observed in the mixed layer of the WTSP during stratified conditions in the absence of significant nitrogen sources other than N_2 fixation. The pertinence of the b_{bp} *vs* PON (POP) relationships should be investigated in other oligotrophic areas, but also in other trophic regimes. This new relationship also opens a promising avenue to assess PON (POP) from ocean color remote sensing using various existing inverse methods [65–67].

Funding

Centre National de la Recherche Scientifique (ANR-14-CE01-0007-01).

Optics EXPRESS

Acknowledgments

The authors thank the crew of the RV *L'Atalante* for outstanding shipboard operations. Gilles Rougier and Marc Picheral are warmly thanked for their efficient help in CTD rosette management and data processing, as well as Catherine Schmechtig for the LEFE-CyBER database management. All data and metadata are available at the following web address: http://www.obs-vlfr.fr/proof/php/outpace/outpace.php. The Argo data were collected and made freely available by the International Argo Project and the national programmes that contribute to it (http://www.argo.ucsd.edu, http://argo.jcommops.org). Argo is a pilot programme of the Global Ocean Observing System. The authors would like to acknowledge Sandra Helias Nunige and Karine Leblanc for providing particulate organic concentrations.

This is a contribution of the OUTPACE (Oligotrophy from Ultra-oligoTrophy PACific Experiment) project (https://outpace.mio.univ-amu.fr/) funded by the French research national agency (ANR-14-CE01-0007-01), the LEFE-CyBER program (CNRS-INSU), the GOPS program (IRD), the CNES, and from the European FEDER Fund under project 1166-39417. The OUTPACE cruise (http://dx.doi.org/10.17600/15000900) was managed by the MIO (OSU Institut Pytheas, AMU, CNRS) from Marseilles (France)

Disclosures

The authors declare no conflicts of interest.

References

1. P. Raimbault, N. Garcia, and F. Cerutti, "Distribution of inorganic and organic nutrients in the South Pacific Ocean – evidence for long-term accumulation of organic matter in nitrogen-depleted waters," Biogeosciences **5**(2), 281–298 (2008).
2. A. Morel, H. Claustre, and B. Gentili, "The most oligotrophic subtropical zones of the global ocean: Similarities and differences in terms of chlorophyll and yellow substance," Biogeosciences **7**(10), 3139–3151 (2010).
3. R. C. Dugdale, D. W. Menzel, and J. H. Ryther, "Nitrogen fixation in the Sargasso Sea," Deep Sea Res., Part I **7**(4), 297–300 (1961).
4. D. Karl, A. Michaels, B. Bergman, D. Capone, E. Carpenter, R. Letelier, F. Lipschultz, H. Paerl, D. Sigman, and L. Stal, "Dinitrogen fixation in the world's oceans," Biogeochemistry **57**(1), 47–98 (2002).
5. S. Bonnet, M. Caffin, H. Berthelot, and T. Moutin, "Hot spot of N_2 fixation in the western tropical South Pacific pleads for a spatial decoupling between N_2 fixation and denitrification," Proc. Natl. Acad. Sci. U. S. A. **114**(14), E2800–E2801 (2017).
6. T. Moutin, T. Wagener, M. Caffin, A. Fumenia, A. Gimenez, M. Baklouti, P. Bouruet-Aubertot, M. Pujo-Pay, K. Leblanc, D. Lefevre, S. Helias Nunige, N. Leblond, O. Grosso, and A. de Verneil, "Nutrient availability and the ultimate control of the biological carbon pump in the Western Tropical South Pacific Ocean," Biogeosciences **15**(9), 2961–2989 (2018).
7. A. Gimenez, M. Baklouti, T. Wagener, and T. Moutin, "Diazotrophy as the main driver of the oligotrophy gradient in the western tropical South Pacific Ocean: results from a one-dimensional biogeochemical–physical coupled model," Biogeosciences **15**(21), 6573–6589 (2018).
8. D. Roemmich, M. H. Alford, H. Claustre, K. Johnson, B. King, J. Moum, and M. Scanderbeg, "On the Future of Argo: A Global, Full-Depth, Multi-Disciplinary Array," Front. Mar. Sci. **6**, 439 (2019).
9. K. S. Johnson, J. N. Plant, L. J. Coletti, H. W. Jannasch, C. M. Sakamoto, S. C. Riser, D. D. Swift, N. L. Williams, E. Boss, N. Haentjens, L. D. Talley, and J. L. Sarmiento, "Biogeochemical sensor performance in the SOCCOM profiling float array," J. Geophys. Res.: Oceans **122**(8), 6416–6436 (2017).
10. J. J. Cullen, "The Deep Chlorophyll Maximum: Comparing Vertical Profiles of Chlorophyll a," Can. J. Fish. Aquat. Sci. **39**(5), 791–803 (1982).
11. D. A. Siegel, M. J. Behrenfeld, S. Maritorena, C. R. McClain, D. Antoine, S. W. Bayley, P. S. Bontempi, E. S. Boss, H. M. Dierssen, S. C. Doney, R. E. Eplee Jr, R. H. Evans, G. C. Feldman, A. Fields, B. A. Franz, N. A. Kuring, C. Mengelt, N. B. Nelson, F. S. Patt, W. D. Robinson, J. L. Sarmiento, C. M. Swan, P. J. Werdell, T. K. Westberry, J. G. Wilding, and J. A. Yoder, "Regional to global assessments of phytoplankton dynamics from the SeaWiFS mission," Remote Sens. Environ. **135**, 77–91 (2013).
12. D. Stramski, E. Boss, D. Bogucki, and K. J. Voss, "The role of seawater constituents in light backscattering in the ocean," Prog. Oceanogr. **61**(1), 27–56 (2004).
13. X. Xing, G. Qiu, E. Boss, and H. Wang, "Temporal and vertical variations of particulate and dissolved optical properties in the South China Sea," J. Geophys. Res.: Oceans **124**(6), 3779–3795 (2019).

Optics EXPRESS

14. D. Stramski, "Refractive index of planktonic cells as a measure of cellular carbon and chlorophyll a content," Deep Sea Res., Part I **46**(2), 335–351 (1999).
15. D. Stramski, R. A. Reynolds, M. Babin, S. Kaczmarek, M. R. Lewis, R. Rottgers, A. Sciandra, M. Stramska, M. S. Twardowski, B. A. Franz, and H. Claustre, "Relationships between the surface concentration of particulate organic carbon and optical properties in the eastern South Pacific and eastern Atlantic Oceans," Biogeosciences **5**(1), 171–201 (2008).
16. H. Loisel, E. Bosc, D. Stramski, K. Oubelkheir, and P. Y. Deschamps, "Seasonal variability of the backscattering coefficient in the Mediterranean Sea based on Satellite SeaWiFS imagery," Geophys. Res. Lett. **28**(22), 4203–4206 (2001).
17. H. Loisel, J. M. Nicolas, P. Y. Deschamps, and R. Frouin, "Seasonal and inter-annual variability of particulate organic matter in the global ocean," Geophys. Res. Lett. **29**(24), 49-1–49-4 (2002).
18. L. Duforêt-Gaurier, H. Loisel, D. Dessailly, K. Nordkvist, and S. Alvain, "Estimates of particulate organic carbon over the euphotic depth from in situ measurements: Application to satellite data over the global ocean," Deep Sea Res., Part I **57**(3), 351–367 (2010).
19. I. Cetinić, M. J. Perry, N. T. Briggs, E. Kallin, E. A. D'Asaro, and C. M. Lee, "Particulate organic carbon and inherent optical properties during 2008 North Atlantic Bloom Experiment," J. Geophys. Res. **117**(C6), C06028(2012).
20. S. B. Moran, M. A. Charette, S. M. Pike, and C. A. Wicklund, "Differences in seawater particulate organic carbon concentration in samples collected using small-and large-volume methods: the importance of DOC adsorption to the filter blank," Mar. Chem. **67**(1-2), 33–42 (1999).
21. W. D. Gardner, M. J. Richardson, C. A. Carlson, D. Hansell, and A. V. Mishonov, "Determining true particulate organic carbon: bottles, pumps and methodologies," Deep Sea Res., Part II **50**(3-4), 655–674 (2003).
22. Z. Liu, G. Stewart, J. K. Cochran, C. Lee, R. A. Armstrong, D. J. Hirschberg, B. Gasser, and J. C. Miquel, "Why do POC concentrations measured using Niskin bottle collections sometimes differ from those using in-situ pumps?" Deep Sea Res., Part I **52**(7), 1324–1344 (2005).
23. P. Raimbault, F. Diaz, W. Pouvesle, and B. Boudjellal, "Simultaneous determination of particulate organic carbon, nitrogen and phosphorus collected on filters, using a semi-automatic wet-oxidation method," Mar. Ecol.: Prog. Ser. **180**, 289–295 (1999).
24. D. V. Hebel and D. M. Karl, "Seasonal, interannual and decadal variations in particulate matter concentrations and composition in the subtropical North Pacific Ocean," Deep Sea Res., Part II **48**(8-9), 1669–1695 (2001).
25. S. Bonnet, M. Caffin, H. Berthelot, O. Grosso, M. Benavides, S. Helias-Nunige, C. Guieu, M. Stenegren, and R. A. Foster, "In-depth characterization of diazotroph activity across the western tropical South Pacific hotspot of N_2 fixation (OUTPACE cruise)," Biogeosciences **15**(13), 4215–4232 (2018).
26. A. C. Martiny, J. A. Vrugt, and M. W. Lomas, "Concentrations and ratios of particulate organic carbon, nitrogen, and phosphorus in the global ocean," Sci. Data **1**(1), 140048 (2014).
27. T. Moutin, A. M. Doglioli, A. De Verneil, and S. Bonnet, "The Oligotrophy to the UlTra Oligotrophy PACific Experiment (OUTPACE cruise, Feb. 18 to Apr. 3, 2015)," Biogeosciences **14**(13), 3207–3220 (2017).
28. M. Pujo-Pay and P. Raimbault, "Improvement of the wet-oxidation procedure for simultaneous determination of particulate organic nitrogen and phosphorus collected on filters," Mar. Ecol.: Prog. Ser. **105**, 203–207 (1994).
29. A. Aminot and R. Kérouel, Dosage automatique des nutriments dans les eaux marines : méthodes en flux continu, (Ifremer, 2007).
30. L. A. Currie, "Detection and quantification limits: origins and historical overview," Anal. Chim. Acta **391**(2), 127–134 (1999).
31. P. Raimbault and G. S. Slawyk, "A semiautomatic, wet-oxidation method for the determination of particulate organic nitrogen collected on filters," Limnol. Oceanogr.: Methods **36**(2), 405–408 (1991).
32. A. Wong, R. Keeley, and T. Carval, "Argo quality control manual," *Argo Data Management* 1–50 (2013).
33. C. Schmechtig, H. Claustre, A. Poteau, and F. D'Ortenzio, "Bio-Argo quality control manual for the Chlorophyll-A concentration", (2018).
34. C. Schmechtig, E. Boss, N. Briggs, H. Claustre, G. Dall'Olmo, and A. Poteau, "BGC Argo quality control manual for particles backscattering", (2019).
35. C. G. de Boyer Montegut, A. S. Madec, A. Fischer, A. Lazar, and D. Iudicone, "Mixed layer depth over the global ocean: An examination of profile data and a profile-based climatology," J. Geophys. Res.: Oceans **109**(C12), C12003 (2004).
36. C. Roesler, J. Uitz, H. Claustre, E. Boss, X. Xing, E. Organelli, N. Briggs, A. Bricaud, C. Schmechtig, A. Poteau, F. D'Ortenzio, J. Ras, S. Drapeau, N. Haëntjens, and M. Barbieux, "Recommendations for obtaining unbiased chlorophyll estimates from in situ chlorophyll fluorometers: A global analysis of WET Labs ECO sensors," Limnol. Oceanogr.: Methods **15**(6), 572–585 (2017).
37. J. Sullivan, M. Twardowski, S. Ronald, J. V. Zaneveld, and C. C. Moore, Measuring optical backscattering in water, Light scattering reviews 7, pp. 189–224. (Springer Kokhanovsky, Berlin, Germany, 2013).
38. N. Bock, F. V. Wambeke, M. Dion, and S. Duhamel, "Microbial community structure in the western tropical South Pacific," Biogeosciences **15**(12), 3909–3925 (2018).
39. V. Martinez-Vicente, G. Dall'Olmo, G. Tarran, E. Boss, and S. Sathyendranath, "Optical backscattering is correlated with phytoplankton carbon across the Atlantic Ocean," Geophys. Res. Lett. **40**(6), 1154–1158 (2013).

Optics EXPRESS

40. R. M. Letelier, R. Bidigare, D. V. Hebel, M. Ondrusek, C. D. Winn, and D. M. Karl, "Temporal variability of phytoplankton community structure-based on pigment analysis," Limnol. Oceanogr. **38**(7), 1420–1437 (1993).
41. C. D. Winn, J. Campbell, J. R. Christian, R. M. Letelier, D. V. Hebel, J. E. Dore, L. Fujieki, and D. M. Karl, "Seasonal variability in the phytoplankton community of the north pacific subtropical gyre," Global Biogeochem. Cycles **9**(4), 605–620 (1995).
42. S. Blain S, S. Bonnet, and C. Guieu, "Dissolved iron distribution in the tropical and subtropical South Eastern Pacific," Biogeosciences **5**(1), 269–280 (2008).
43. T. Moutin, D. M. Karl, S. Duhamel, P. Rimmelin, P. Raimbault, B. A. S. Van Mooy, and H. Claustre, "Phosphate availability and the ultimate control of new nitrogen," Biogeosciences **5**(1), 95–109 (2008).
44. R. A. Reynolds, D. Stramski, and B. G. Mitchell, "A chlorophyll-dependent semi analytical model derived from field measurements of absorption and backscattering coefficients within the Southern Ocean," J. Geophys. Res.: Oceans **106**(C4), 7125–7138 (2001).
45. T. K. Westberry, G. Dall'Olmo, E. Boss, M. J. Behrenfeld, and T. Moutin, "Coherence of particulate beam attenuation and backscattering coefficients in diverse open ocean environments," Opt. Express **18**(15), 15419–15425 (2010).
46. Y. Huot, A. Morel, M. S. Twardowski, D. Stramski, and R. A. Reynolds, "Particle optical backscattering along a chlorophyll gradient in the upper layer of the eastern South Pacific Ocean," Biogeosciences **5**(2), 495–507 (2008).
47. M. Barbieux, J. Uitz, A. Bricaud, E. Organelli, A. Poteau, C. Schmechtig, B. Gentilli, G. Obolensky, E. Leymarie, C. Penkerc'h, F. D'Ortenzio, and H. Claustre, "Assessing the variability in the relationship between the particulate backscattering coefficient and the chlorophyll a concentration from a global Biogeochemical-Argo database," J. Geophys. Res.: Oceans **123**(2), 1229–1250 (2018).
48. A. de Verneil, L. Rousselet, A. M. Doglioli, A. A. Petrenko, and T. Moutin, "The fate of a southwest Pacific bloom: gauging the impact of submesoscale vs. mesoscale circulation on biological gradients in the subtropics," Biogeosciences **14**(14), 3471–3486 (2017).
49. T. Wagener, C. Guieu, R. Losno, S. Bonnet, and N. Mahowald, "Revisiting atmospheric dust export to the Southern Hemisphere ocean: Biogeochemical implications," Global Biogeochem. Cycles **22**(2), GB2006 (2008).
50. D. J. McGillicuddy, L. A. Anderson, N. R. Bates, T. Bibby, K. O. Buesseler, C. A. Carlson, and D. A. Hansell, "Eddy/wind interactions stimulate extraordinary mid-ocean plankton blooms," Science **316**(5827), 1021–1026 (2007).
51. C. S. Law, E. M. S. Woodward, M. J. Ellwood, A. Marriner, S. J. Bury, and K. A. Safi, "Response of surface nutrient inventories and nitrogen fixation to a tropical cyclone in the southwest Pacific," Limnol. Oceanogr. **56**(4), 1372–1385 (2011).
52. H. Berthelot, T. Moutin, S. L'Helguen, K. Leblanc, S. Hélias, O. Grosso, N. Leblond, B. Charrière, and S. Bonnet, "Dinitrogen fixation and dissolved organic nitrogen fueled primary production and particulate export during the VAHINE mesocosm experiment (New Caledonia lagoon)," Biogeosciences **12**(13), 4099–4112 (2015).
53. M. Caffin, H. Berthelot, V. Cornet-Barthaux, A. Barani, and S. Bonnet, "Transfer of diazotroph-derived nitrogen to the planktonic food web across gradients of N_2 fixation activity and diversity in the western tropical South Pacific Ocean," Biogeosciences **15**(12), 3795–3810 (2018).
54. A. C. Martiny, J. A. Vrugt, F. W. Primeau, and M. W. Lomas, "Regional variation in the particulate organic carbon to nitrogen ratio in the surface ocean," Global Biogeochem. Cycles **27**(3), 723–731 (2013).
55. P. G. Falkowski, "Evolution of the nitrogen cycle and its influence on the biological sequestration of CO_2 in the ocean," Nature **387**(6630), 272–275 (1997).
56. C. M. Moore, M. M. Mills, K. R. Arrigo, I. Berman-Frank, L. Bopp, P. W. Boyd, E. D. Galbraith, R. J. Geider, C. Guieu, S. L. Jaccard, T. D. Jickells, J. La Roche, T. M. Lenton, N. M. Mahowald, E. Marañón, I. Marinov, J. K. Moore, T. Nakatsuka, A. Oschlies, M. A. Saito, T. F. Thingstad, A. Tsuda, and O. Ulloa, "Processes and patterns of oceanic nutrient limitation," Nat. Geosci. **6**(9), 701–710 (2013).
57. E. D. Galbraith and A. C. Martiny, "A simple nutrient-dependence mechanism for predicting the stoichiometry of marine ecosystems," Proc. Natl. Acad. Sci. **112**(27), 8199–8204 (2015).
58. R. J. Geider and J. La Roche, "Redfield revisited: variability of C:N:P in marine microalgae and its biochemical basis," Eur. J. Phycol. **37**(1), 1–17 (2002).
59. S. Duhamel, T. Moutin, F. Van Wambeke, B. Van Mooy, P. Rimmelin, and H. Claustre, "Claustre Growth and specific P-uptake rates of bacterial and phytoplanktonic communities in the Southeast Pacific (BIOSOPE cruise)," Biogeosciences **4**(6), 941–956 (2007).
60. D. W. Menzel and J. H. Ryther, "The composition of particulate organic matter in the western north Atlantic," Limnol. Oceanogr. **9**(2), 179–186 (1964).
61. A. Paytan, B. J. Cade-Menun, K. McLaughlin, and K. L. Faul, "Selective phosphorus regeneration of sinking marine particles: evidence from 31P-NMR," Mar. Chem. **82**(1-2), 55–70 (2003).
62. B. Schneider, R. Schlitzer, G. Fischer, and E. M. Nöthig, "Depth-dependent elemental compositions of particulate organic matter (POM) in the ocean," Global Biogeochem. Cycles **17**(2), 1032 (2003).
63. V. Martinez-Vicente, G. H. Tilstone, S. Sathyendranath, P. I. Miller, and S. B. Groom, "Contributions of phytoplankton and bacteria to the optical backscattering coefficient over the Mid-Atlantic Ridge," Mar. Ecol.: Prog. Ser. **445**, 37–51 (2012).
64. J. R. Graff, T. K. Westberry, A. J. Milligan, M. B. Brown, G. Dall'Olmo, V. van Dongen-Vogels, K. M. Reifel, and J. B. Behrenfeld, "Analytical phytoplankton carbon measurements spanning diverse ecosystems," Deep Sea Res., Part I **102**, 16–25 (2015).

Optics EXPRESS

65. Z. P. Lee, K. L. Carder, and R. Arnone, "Deriving inherent optical properties from water color: A multi-band quasi-analytical algorithm for optically deep waters," Appl. Opt. **41**(27), 5755–5772 (2002).
66. P. J. Werdell, B. A. Franz, S. W. Bailey, G. W. Feldman, E. Boss, V. E. Brando, and A. Mangin, "Generalized ocean color inversion model for retrieving marine inherent optical properties," Appl. Opt. **52**(10), 2019–2037 (2013).
67. H. Loisel, D. Stramski, D. Dessailly, C. Jamet, L. Li, and R. A. Reynolds, "An inverse model for estimating the optical absorption and backscattering coefficients of seawater from remote-sensing reflectance over a broad range of oceanic and coastal marine environments," J. Geophys. Res.: Oceans **123**(3), 2141–2171 (2018).